Available online at **www.joac.info**

ISSN: 2278-1862

Journal of Applicable Chemistry

2019, 8 (1): 419-424

(International Peer Reviewed Journal)

Visible light Responsive Photocatalytic Activity of Pd/Fe_2O_3 Nanoparticles for Congo Red dye Degradation

Challarapu Venkataramana*, R. Balaji Anjaneyulu, Jhansi Rani Sunkara and R. Muralikrishna

Department of Physical, Nuclear Chemistry and Chemical Oceanography,
Andhra University, Visakhapatnam, **INDIA**
Email: venkatau17@gmail.com

Accepted on 16th January, 2019

ABSTRACT

The Photocatalytic activity of hydrothermal synthesized Pd/Fe_2O_3 nanoparticles on Congo red dye degradation was presented in this paper. The phase, functionality, structural and morphological features of prepared nanoparticles were characterized by X-ray diffraction (XRD), Fourier transform infrared Spectroscopy (FTIR), scanning electron microscopy (SEM) and surface area was measured by Brunauer-Emmett-Teller (BET) analysis. The photocatalytic activity of as-synthesized materials was determined by degradation efficiency of Congo red, and the results show that Pd/Fe_2O_3 nanoparticles exhibits higher photodegradation activity than Fe_2O_3 nanoparticles.

Graphical Abstract

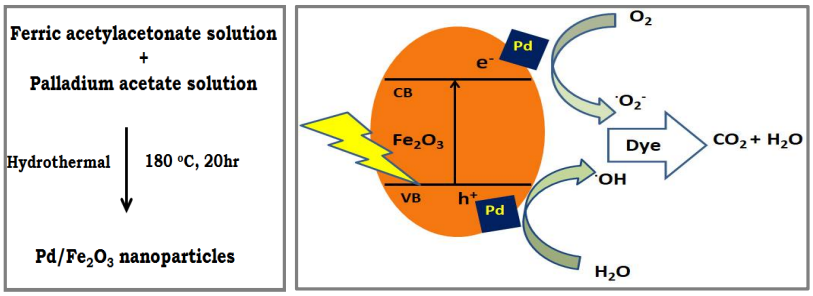

Schematic diagram of a possible photocatalysis mechanism.

Keywords: Hydrothermal, Pd/Fe_2O_3 nanoparticles, Congo red and Photocatalysis.

INTRODUCTION

Photo-assisted catalysis over a solid semiconductor has been recognized as a promising approach for the elimination of many organic pollutants [**1–3**]. The organic molecules, after adsorbed on the catalyst surface, are mineralized into carbon dioxide and water through a redox reaction by hydroxyl radicals or superoxide radicals. These photo-excited active species were produced when water reacts with holes in valence band and oxygen with electrons in conduction band.

Oxides of transition metals are widely used as photocatalysts, but the activity decline is frequently encountered because of the electron-hole charge recombination on the surface of oxides within nanoseconds [**4**]. To circumvent this problem, depositing a noble metal on a metal oxide as support is employed [**5, 6**]. This metal supported metal oxide is beneficial to photocatalysis due to its role of inhibiting the electron–hole recombination [**7**]. One of the transition metal oxide, Fe_2O_3 has paid intensive attention due to its stability, eco-friendly, high efficiency, non-toxic and inexpensive [**8, 9**]. Fe_2O_3 is n-type semiconducting with an indirect band gap of ~2.2 eV and it has attractive wide applications in pigment, gas sensors and catalysis [**10–12**]. In the present work, Fe_2O_3 and Pd/Fe_2O_3 nanoparticles are prepared via hydrothermal route, the photocatalytic activity was evaluated on the basis of degradation of Congo red (CR) dye.

MATERIALS AND METHODS

Ferric acetylacetonate ($C_{15}H_{21}FeO_6$), Palladium acetate ($C_4H_6O_4Pd$) and Ethanol were purchased from Merck Chemicals Pvt. Ltd, India. CR was procured from Rankem Chemicals Pvt. Ltd, India. The two solutions were prepared separately by dissolving in ethanol, the equal ratio of the solutions was mixed slowly and allowed to stir for12 h, the obtained reddish- brown solution was transferred into a Teflon-lined hydrothermal autoclave, which was maintained at 180°C for 20 h. The autoclave was allowed to cool to room temperature; the obtained precipitate was washed several times with absolute ethanol and double-distilled (2D) water and then dried overnight at 60°C. Same procedure was followed for the preparation of pure Fe_2O_3 nanoparticles.

Instrumentation: Crystal phase identification of the synthesized photocatalysts was characterized by X-ray-powder diffraction (XRD) using graphite monochromatized Cu Kα radiation. The XRD patterns were obtained in the range of 10°–80° (2θ) at a scanning rate of 0.02° S^{-1}. Fourier Transform Infrared (FTIR) spectra were recorded on a FTIR analyzer. Surface morphology and distribution of particles were studied by scanning electron microscope (SEM) with an acceleration voltage of 15 keV. The surface areas of the samples were calculated by the Brunauer–Emmett–Teller (BET).

Photocatalytic process: To evaluate the photocatalytic abilities of the as-prepared Fe_2O_3 and Pd/Fe_2O_3 nanoparticles, CR was used as the hypothesized organic pollutant in our study. All the reactions were performed at room temperature and atmospheric pressure. Typically, 100 mg of the catalyst were suspended in 100 mL dye solution (25 mg L^{-1}) in a 150 mL beaker. Prior to irradiation, the system was placed in dark environment and stirred for 10 min until adsorption-desorption equilibrium was reached. Following this, the photocatalytic reaction was started by the exposure of visible light. After exposure to visible light (400W metal halide lamp), certain mixture solution was taken out at regular intervals and centrifuged to remove the catalyst. The photodegradation efficiency was monitored by measuring the absorbance using UV-Vis spectroscopy (Shimadzu, UV-1800) at room temperature, using a quartz microcell. The photometric analysis of the all photocatalyst samples before and after irradiation can be used by measuring % of degradation (Degradation efficiency (DE %)). Defined the following equation (1), where C_0 is the initial concentration of dye and C_t is the concentration of dye after irradiation of the samples in desired time intervals. All samples were conducted under the same experimental conditions.

$$\text{Degradation efficiency (DE\%)} = \frac{C_0 - C_t}{C_0} \times 100 \qquad -(1)$$

RESULTS AND DISCUSSION

The XRD patterns of Fe_2O_3 and Pd/ Fe_2O_3nanoparticles are shown in figure 1. The Fe_2O_3 spectrum shows diffraction peaks at 2θ = 24.2°, 33.1°, 35.7°, 40.9°, 49.4°, 54.2°, 57.6°, 62.4°, 64.0°, 69.6°, 72.0° and 75.5° assigned to the (012), (104), (110), (113), (024), (116), (122), (214), (300), (208),

(101) and (220) diffraction planes respectively (JCPDS, no. 33-0664), which are attributed to pure Fe_2O_3 nanoparticles [13]. In Pd/ Fe_2O_3 spectrum shows dominant diffraction peaks at 2θ = 40.3°, 46.5° and 68.7° assigned to the (111), (200) and (311) were attributed to the Pd nanoparticles (JCPDS no. 87-0638) [14], which indicating the formation of pure phase Pd/Fe_2O_3 nanocrystals by hydrothermal synthesis.

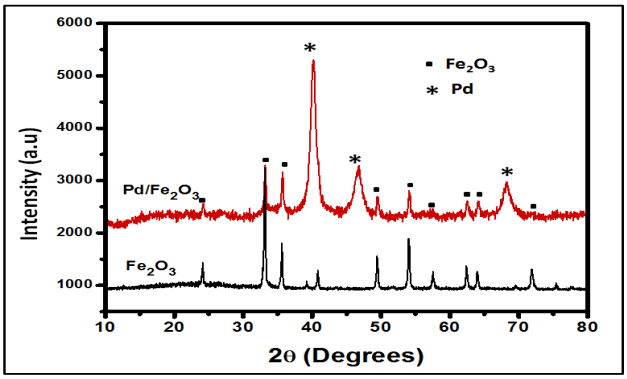

Figure 1. XRDspectra of Fe_2O_3 and Pd/Fe_2O_3 nanoparticles.

Figure 2 shows the FTIR spectra of Fe_2O_3 and Pd/ Fe_2O_3 nanoparticles. The bands centered at 3357 and 1375 cm^{-1} are ascribed to O-H bonding stretching and bending vibrational modes [15]. It suggests the presence of very small amount of free and adsorbed water on the surface of the samples. As shown in figure, a peak nearly 500 cm^{-1} is ascribed to the stretching between iron and oxygen in Fe_2O_3 and supported metal (Pd)–oxygen stretching modes. Similar observations have been documented in literature [16]. On adding supporting metal, the band at 500 cm^{-1} shifts toward slightly lower frequency suggesting the possible formation of Pd/ Fe_2O_3 nanoparticles.

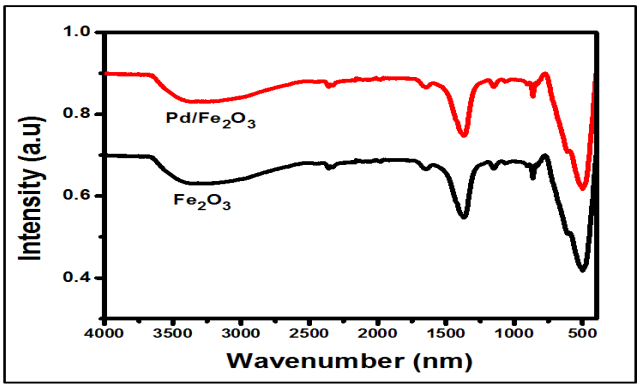

Figure 2. FTIR spectra of Fe_2O_3 and Pd/Fe_2O_3 nanoparticles.

Structure and morphological features of synthesized samples were examined by scanning electron microscopy (SEM). Figure 3 shows pure Fe_2O_3 and Pd/Fe_2O_3 nanoparticles. The SEM images demonstrate that the homogeneous and stone like agglomerates. There is no significant morphological difference among the Fe_2O_3 and Pd/Fe_2O_3, i.e. the supporting of Pd into Fe_2O_3does not influence the morphology. In Pd/Fe_2O_3 images shows Pd particles are well decorated on the surface of the Fe_2O_3 nanoparticles, which indicates formation of Pd/Fe_2O_3 nanoparticles via synthesis route. The morphological analysis supports the XRD, which confirm the pure form of Pd/Fe_2O_3 nanoparticles.
N_2 adsorption/desorption isotherms of Fe_2O_3, Pd/Fe_2O_3 are shown in table 1. The results show that the BET surface area of Pd/Fe_2O_3 higher thanFe_2O_3. The higher surface area of Pd/Fe_2O_3 would be beneficial to adsorb more organic pollutants on its surface, which consequently enhances the reaction rate of degradation.

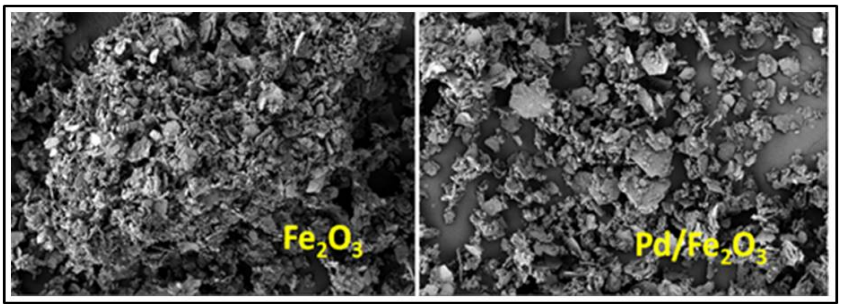

Figure 3. SEM images of Fe_2O_3 and Pd/Fe_2O_3 nanoparticles.

Table 1. BET surface areas of Fe_2O_3 and Pd/Fe_2O_3 nanoparticles

S.No	Catalyst	BET surface area (m^2g^{-1})
1	Fe_2O_3	36.50
2	Pd/Fe_2O_3	47.13

Photocatalytic process performance: The photocatalytic activity of Fe_2O_3 and Pd/Fe_2O_3 nanoparticles were examined by degradation of CR aqueous solution under visible light illumination. Figure 4(A) and 4(B) reveals the temporal evolution of the UV-visible absorption spectra of CR

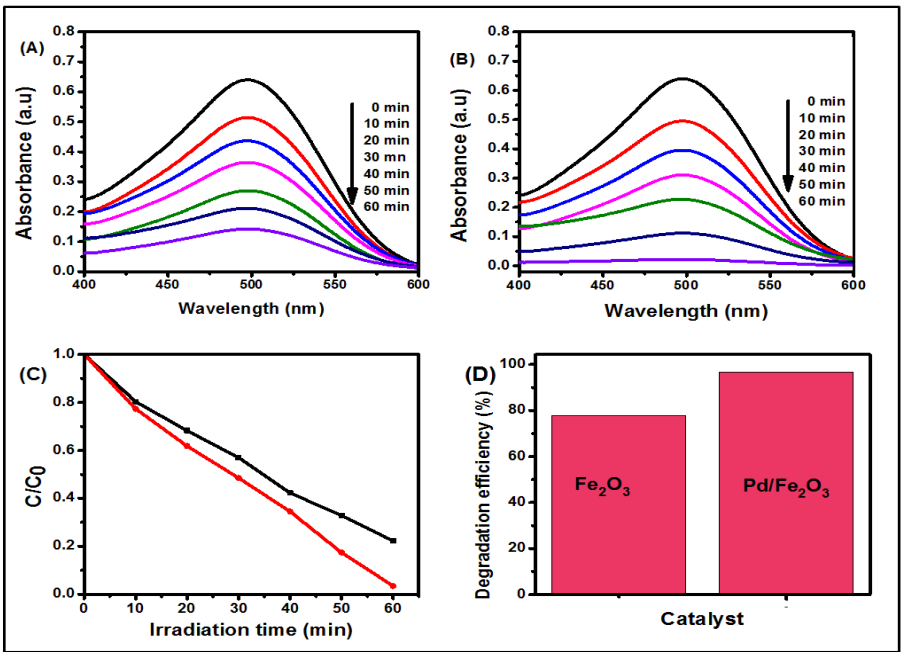

Figure 4. (A) and (B) UV-Visible absorption spectral changes of CR during photocatalytic degradation by Fe_2O_3 and Pd/Fe_2O_3 nanoparticles. (C) Photocatalytic degradation of CR using Fe_2O_3 and Pd/Fe_2O_3 nanoparticles under visible light illumination. (D) The degradation efficiency of CR induced by Fe_2O_3 and Pd/Fe_2O_3 nanoparticles.

degraded over the Fe_2O_3 and Pd/Fe_2O_3 nanoparticles and figure 4(C) shows the effect of visible light irradiation time (t) on the normalized CR concentration (C_t/C_0) for the CR aqueous solutions containing both Fe_2O_3 and Pd/Fe_2O_3 nanoparticles. After irradiation of 60 min, the photocatalytic degradation efficiency was calculated and the efficiency is 77.8 and 96.6% for Fe_2O_3 and Pd/Fe_2O_3 nanoparticles respectively (Figure 4D). It shows that the degradation efficiency of CR after 60 min, visible light irradiation, increases monotonically with Pd loading, due to more surface area (Table 1) and more visible light response.

The highest photocatalytic activity of Pd/Fe_2O_3nanoparticles is due to the presence of metallic Pd particles on the iron oxide surface. On irradiation of visible light, the Pd nanoparticles act as the sites for electron accumulation, the better separation between electrons and holes formation [**17, 18**], thus enhancing the photocatalytic activity. The possible mechanism (Figure 5) for photocatalytic degradation of dye in the presence of Pd/Fe_2O_3 nanoparticles under visible light irradiation can be shown by the following equations. Based on the experimental results, Pd/Fe_2O_3 nanoparticles exhibit the highest photocatalytic activity than the Fe_2O_3 nanoparticles.

$$Pd/Fe_2O_3 + h\upsilon \longrightarrow Pd/Fe_2O_3(h^+) + Pd/Fe_2O_3(e^-)$$

$$Pd/Fe_2O_3(h^+) + H_2O \longrightarrow Pd/Fe_2O_3 + {}^{\bullet}OH + H^+$$

$$Pd/Fe_2O_3(e^-) + O_2 \longrightarrow Pd/Fe_2O_3 + {}^{\bullet}O_2^-$$

$$^{\bullet}OH/{}^{\bullet}O_2^- + Dye \longrightarrow CO_2 + H_2O$$

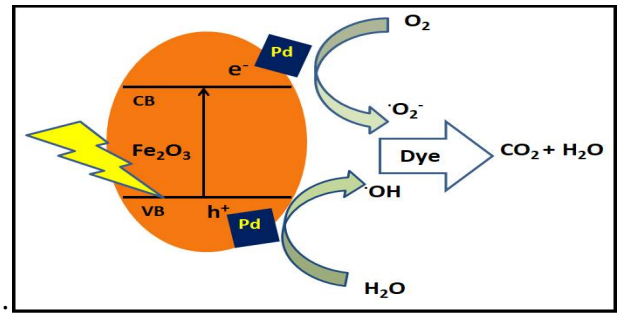

Figure 5. Schematic diagram of a possible photocatalysis mechanism.

APPLICATION

Superior photocatalytic activity for the Pd/Fe_2O_3 nanoparticles was observed compared to Fe_2O_3 nanoparticles. The results have demonstrated the feasibility of Pd/Fe_2O_3 nanoparticles as a model photocatalyst for dye decontamination in wastewater.

CONCLUSION

Herein, we synthesized of Pd/Fe_2O_3 nanoparticles via hydrothermal route. The structure and morphology of synthesized Pd/Fe_2O_3 nanoparticles was studied using various instrumental techniques. The photocatalytic activity of as-prepared Pd/Fe_2O_3 nanoparticles was measured using the degradation of CR dye. We have observed superior photocatalytic activity for the Pd/Fe_2O_3 nanoparticles compared toFe_2O_3 nanoparticles. The results have demonstrated the feasibility of Pd/Fe_2O_3 nanoparticles as a model photocatalyst for dye decontamination in wastewater.

ACKNOWLEDGEMENTS

Ch. Venkataramana acknowledges to Council of Scientific and Industrial Research (CSIR), New Delhi, India for the financially support and sincere thanks to the administration of Andhra University, Visakhapatnam for extending its cooperation in carrying out this work.

Conflicts of interest: The authors declared that there is no any conflict of interest.

REFERENCES

[1]. R. Comparelli, E. Fanizza, M. L. Curri, P. D. Cozzoli, G. Mascolo, R. Passino, A. Agostiano, *Appl. Catal. B: Environ.*, **2005**, 55, 81.
[2]. C. Galindo, P. Jacques, A. Kalt, *J. Photochem. Photobiol. A: Chem*., **2000**, 130, 35.
[3]. E. Stathatos, T. Petrova, P. Lianos, *Langmuir*, **2001**, 17, 5025.
[4]. G. Rothenberger, J. Moser, M. Gratzel, N. Serpone, D. K. Sharma, *J. Am. Chem. Soc.*, **1985**, 107, 8054.
[5]. W. Dirk, *Thermochim. Acta*, **2006**, 44, 195–199.
[6]. J. Chen, L.N. Xu, W.Y. Li, *Adv. Mater*., **2005**, 17, 582–586.
[7]. I. K. Konstantinou, T. A. Albanis, *Appl. Catal. B: Environ.*, **2004**, 49, 1.
[8]. M. Barroso, A. J. Cowan, S. R. Pendlebury, M. Grätzel, D. R. Klug, J. R. Durrant, *J. Am. Chem. Soc.*, **2011**, 133, 14868–14871.
[9]. J. Gu, S. Li, E. Wang, Q. Li, G. Sun, R. Xu, H. Zhang, *J. Solid State Chem.*, **2009**, 182, 1265–1272.
[10]. S. Osama, R. Wolfgang, S. Achim, K. Grigorios, S. Robert, *Angew. Chem. Int. Ed*., **2003**, 42, 5760–5763.
[11]. E. Stathatos, T. Petrova, P. Lianos, *Langmuir*, **2001**, 17, 5025.
[12]. H. M. Sung-Suh, J. R. Choi, H. J. Hah, S. M. Koo, Y. C. Bae, *J. Photochem. Photobiol. A: Chem*., **2004**, 163, 37.
[13]. S. B. Wang, W. Wang, P. Zhan, S.Q. Jiao, *Chem Electro Chem*., **2014**, 1, 1636-1639.
[14]. S. Navaladian, B. Viswanathan, T. K. Varadarajan, R. P. Viswanath, *Nanoscale Res Lett*., **2008**, 65-71.
[15]. L. M. Song, S. J. Zhang, Colloids Surface, *A Physicochem. Eng. Asp*., **2010**, 360, 1-5.
[16]. S. K. Apte, S. D. Naik, *J. Am. Ceram. Soc.*, **2007**, 90, 412–414.
[17]. S. X. Liu, Z. P. Qu, X.W. Han, C. L. Sun, *Catal. Today*, **2004**, 93–95, 877.
[18]. H. M. Sung-Suh, J. R. Choi, H. J. Hah, S. M. Koo, Y. C. Bae, *J. Photochem. Photobiol. A: Chem.*, **2004**, 163, 37.